Strong asymmetrical bias dependence of magnetoresistance in organic spin valves: the role of ferromagnetic/organic interfaces

2014 New J. Phys. 16 013028

(http://iopscience.iop.org/1367-2630/16/1/013028)

New Journal of Physics
The open access journal at the forefront of physics
Deutsche Physikalische Gesellschaft DPG | IOP Institute of Physics

Strong asymmetrical bias dependence of magnetoresistance in organic spin valves: the role of ferromagnetic/organic interfaces

S W Jiang[1], D J Shu[1], L Lin[1], Y J Shi[1], J Shi[2], H F Ding[1], J Du[1], M Wang[1] and D Wu[1,3]

[1] Department of Physics, National Laboratory of Solid State Microstructures, Nanjing University, Nanjing 210093, People's Republic of China
[2] Department of Physics and Astronomy, University of California, Riverside, CA 92521, USA
E-mail: dwu@nju.edu.cn

Received 25 September 2013, revised 17 December 2013
Accepted for publication 16 December 2013
Published 17 January 2014
New Journal of Physics **16** (2014) 013028
doi:10.1088/1367-2630/16/1/013028

Abstract

We report a highly asymmetric magnetoresistance (MR) bias dependence, with the inverse MR peaking at a negative bias and a sign reversal occurring at a positive bias in prototypical $La_{0.7}Sr_{0.3}MnO_3$(LSMO)/Alq_3/Co organic spin valve (OSV) with a tunnel barrier between LSMO and Alq_3. This behavior is in strong contrast with the commonly found inverse MR in entire bias range for LSMO/Alq_3/Co OSVs. The MR bias voltage dependence is independent on the type of the tunnel barrier, either $SrTiO_3$ or Al_2O_3. Together with first-principle calculations, we demonstrate that the strongly hybridized Co d-states with Alq_3 molecules at the interface are responsible for the efficient d-states spin injection and the observed MR bias dependence is originated from the energy dependent density of states of Co d-states. These findings open up new possibilities to engineer interfacial bonding between ferromagnetic materials and a wide variety of molecule selections for the desired spin transport properties.

[3] Author to whom any correspondence should be addressed.

1. Introduction

The emerging field of organic semiconductor (OSC) based spintronics, which exploits the spin along with the charge of the carriers in OSCs, is expected to provide additional functionality and performance for future organic devices, such as spin organic light-emitting diodes and multifunctional organic-based spin valves [1–6]. This stems from the much longer spin-relaxation times of OSCs than those of inorganic counterparts, which allows retaining spin information in these materials [7, 8]. A prototypical example is the vertical organic spin valve (OSV) structure consisting of two ferromagnetic (FM) electrodes, e.g. $La_{0.7}Sr_{0.3}MnO_3$ (LSMO) and Co, separated by a thin tris-(8, hydroxyquinoline) aluminum (Alq_3) layer, in which a magnetoresistance (MR) ratio of ∼40% and a spin diffusion length of ∼45 nm were observed at low temperatures [1]. In the same device structure with a modified top electrode containing FM nanodots on top of organic layer, Sun *et al* [9] showed a very large MR of more than 300% at 10 K. In contrast to OSV devices with a thick organic layer in which spin diffusion is bound to occur [10], in OSV with an ultrathin organic layer serving as a tunnel barrier, a tunneling magnetoresistance (TMR) of up to 300% 2 K [11] and a TMR of a few percent at room temperature [12] were reported as well in Alq_3-based tunnel junctions.

In the most extensively studied OSV structure, i.e. LSMO/Alq_3/Co, a negative or inverse MR, namely, the resistance of two FM electrodes in the parallel configuration (R_P) higher than that in the antiparallel configuration (R_{AP}), is frequently observed [1, 2, 3, 9, 13]. This inverse MR effect exists in the entire bias voltage range and the MR ratio decreases with increasing bias voltage, showing a maximum MR value around zero bias voltage. According to the Jullière model: $\mathrm{MR} = 2P_1P_2/(1 - P_1P_2)$, where P_1 and P_2 are the spin polarization (SP) of two FM electrodes [14], this inverse MR is attributed to the positive SP of LSMO and negative SP of the Co [1]. Recently, it was reported that the insertion of a thin LiF polar layer at FM/OSC interface caused a relative band shift of OSC with respect to the Fermi energy (E_F) of the FM electrodes, resulting in a sign change of the SP of FM and consequently the sign change of MR in OSVs [15]. This phenomenon is due to the extracted spin from OSC depending on the SP of FM electrode at the energy aligned with the OSC's highest occupied molecular orbital (HOMO) energy level. We are motivated by the idea of manipulating the band alignment by inserting a tunnel barrier. In the present study, we insert a $SrTiO_3$ or Al_2O_3 tunnel barrier between LSMO and Alq_3 to tune the sign of SP and corresponding sign of MR. In addition, we employ our newly developed indirect deposition technique proven effective in making pinhole-free organic layers to fabricate OSVs. We found that the MR ratio shows non-monotonous behaviors with increasing negative bias voltage and the sign of the MR changes at a certain positive bias voltage, independent of the type of barriers. The energy dependence of the density-of-states (DOS) and the corresponding SP of Co explains the observed unique bias dependence characteristic in LSMO/tunnel barrier/Alq_3/Co OSVs. The favor of Co d-states injection is attributed to the strong hybridization of Co out-of-plane d-band states with Alq_3 p-states, supported by *ab initio* theoretical calculation of Co/Alq_3 interface. Furthermore, in regular OSVs without any tunnel barrier, only the hybridized Co d-states near the Fermi level are responsible; therefore, the MR is inverted.

2. Experimental

Figure 1(a) shows a schematic view of the device structure. The LSMO films were epitaxially grown on $SrTiO_3$ (001) substrates by pulsed laser deposition (PLD) with a shadow mask.

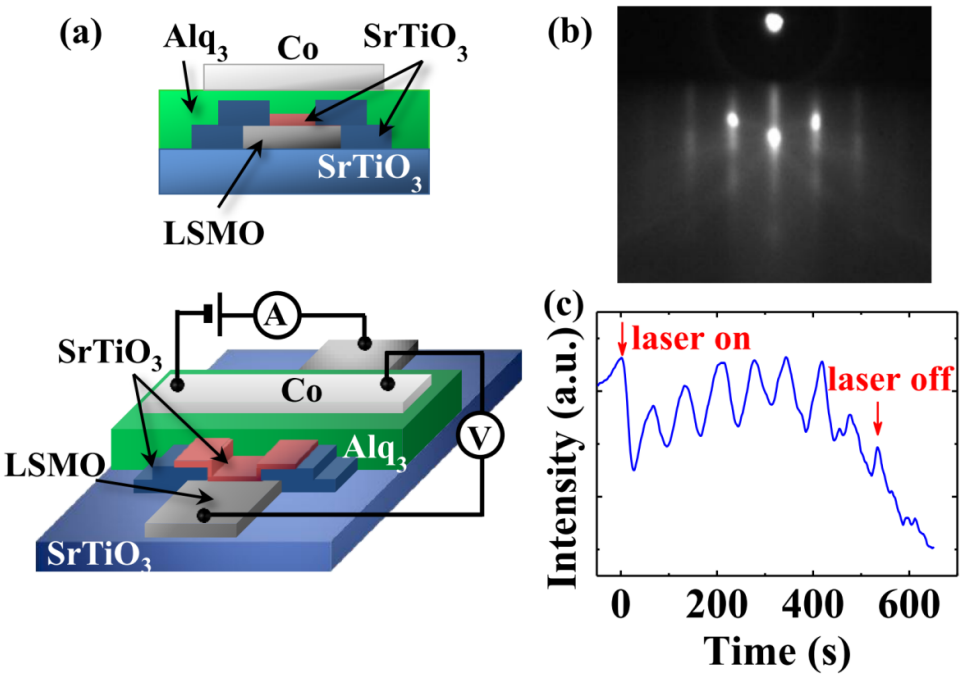

Figure 1. (a) Schematic diagrams of a LSMO/$SrTiO_3$/Alq_3/Co hybrid OSV device. (b) RHEED diffraction pattern of the LSMO film. (c) RHEED oscillation during the growth of the 8 unit cells thick $SrTiO_3$ film on LSMO film.

After growth, the heater was turned off to quench the sample to obtain high quality LSMO films [16]. The PLD grown LSMO film was annealed in oxygen at atmospheric pressure at 1050 °C for 6 h. In order to prevent the possible current leakage at the device edges, ∼100 nm $SrTiO_3$ was epitaxially grown with a shadow mask by PLD to cover the LSMO edges. Then the sample was annealed again in oxygen at atmospheric pressure at 1050 °C for 6 h. An ultra-thin $SrTiO_3$ tunnel barrier was grown on LSMO strip by PLD by applying a KrF-excimer laser at a repetition of 2 Hz and a laser fluency of ∼2 J cm^{-2}. The sample growth temperature and oxygen pressure were 750 °C and 1×10^{-4} Torr, respectively. The growth was monitored *in situ* by reflective high energy electron diffraction (RHEED). A clear RHEED pattern of LSMO film is shown in figure 1(b), indicating that LSMO is a single crystal film. The intensity oscillations of the RHEED spot was observed during $SrTiO_3$ film deposition, shown in figure 1(c), reflecting that the film growth was layer-by-layer. The tunnel barrier thickness was precisely controlled to be 8 unit cells (3.1 nm) based on the oscillation periods. After the growth, the sample was annealed in 1 atm of oxygen at 900 °C for 6 h to further improve the oxidation level.

An Alq_3 film was thermally evaporated at room temperature with a deposition rate of ∼0.07 nm s^{-1} at base pressures of $< 2 \times 10^{-7}$ Torr. The Alq_3 film thickness was measured by a quartz crystal thickness monitor located next to the sample. A thick Alq_3 film (>500 nm) was first fabricated to calibrate the thickness monitor by comparing with the Dekteck150 surface profiler measurements. Atomic force microscopy images confirmed that the morphology of Alq_3 surface grown on $SrTiO_3$, Al_2O_3 or LSMO was very smooth and with the roughness as low as 0.34 nm. One of the critical steps in the fabrication of OSV devices is the top FM layer deposition. It is well known that the top FM deposition can easily cause penetration of FM material into the initially laid down soft organic layer, which consequently results in

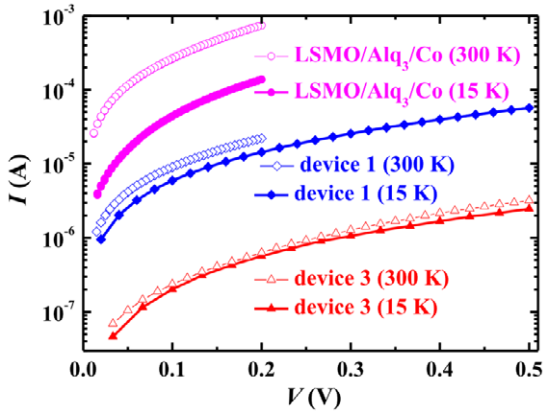

Figure 2. *I–V* curves for LSMO/Alq_3 (50 nm)/Co, device 1 (with $SrTiO_3$ barrier) and device 3 (with Al_2O_3 barrier), respectively, measured at 15 and 300 K.

possible shorts or ill-defined OSC/FM interface [1, 9, 13]. This interface has probably been the most prominent source of poor reproducibility in OSV device fabrication [17, 18]. The indirect deposition method is a remedy of the problem in organic/inorganic hybrid device fabrication. In our case, the top Co electrode was deposited using this method. After the organic layer deposition, the sample surface was *in situ* rotated and formed an opposite facing geometry with respect to the Co source and cooled by liquid nitrogen. The chamber was then back filled with Ar gas to a pressure of 3×10^{-3} Torr from a base pressure of $< 2 \times 10^{-7}$ Torr. During depositing, Co atoms collided with the Ar atoms multiple times and lost their kinetic energy and finally 'softly' landed on top of the organic layer [19]. As the last step, an Al layer was directly deposited on Co to prevent the Co from being oxidized. The active device area was about $0.2 \times 0.2\,mm^2$. In devices using Al_2O_3 as a tunneling barrier, smooth Al_2O_3 was obtained by Ar–O_2 plasma oxidizing a sputter-deposited Al layer [12].

3. Results and discussion

As discussed in the experimental section, we used the indirect deposition method to deposit the top electrode on top of the organic layer. We found it can produce much sharper OSC/FM interfaces and dramatically improve the device yield. In our studies, we fabricated more than ten samples for each type of barriers. Even though the resistance and MR ratio have some variations from sample to sample, we found that the bias dependence characteristics discussed in this work were essentially the same. We believe that the reproducible bias dependence characteristics are more fundamentally related to band structures; therefore, we focus our attention to the overall bias dependence.

Figure 2 displays typical *I–V* characteristics of LSMO (50 nm)/Alq_3 (50 nm)/Co (20 nm)/Al (15 nm), LSMO (50 nm)/$SrTiO_3$ (3.1 nm)/Alq_3 (50 nm)/Co (20 nm)/Al (15 nm) (device 1) and LSMO (50 nm)/Al_2O_3 (∼2.3 nm)/Alq_3 (50 nm)/Co (20 nm)/Al (15 nm) (device 3) in a semi-log plot at 15 and 300 K, respectively. Note that, for comparison, the thickness of the Alq_3 films is the same for all the devices, i.e. the resistance of the Alq_3 films is expected to be the same.

Obviously, the current of the devices with a tunnel barrier ($SrTiO_3$ or Al_2O_3 in device 1 or 3) is significantly lower than that of device with only Alq_3 spacer, indicating that the

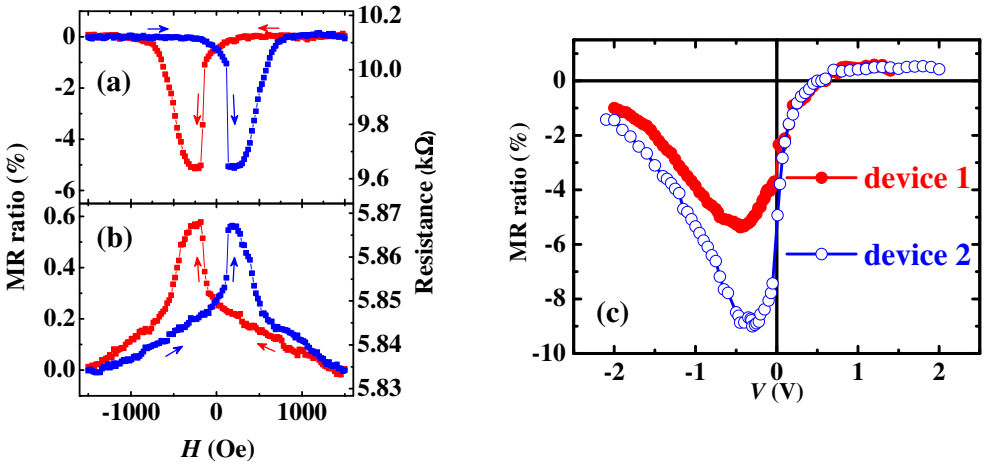

Figure 3. (a) MR loops of device 1 (with $SrTiO_3$ tunneling barrier) measured at 15 K with a bias voltage of −0.44 V. (b) MR loops of device 1 measured at 15 K with a bias voltage of 0.90 V. (c) MR ratio as a function of the applied bias voltage of devices 1 and 2.

total resistance is dominated by the tunnel barrier. In the device without any tunnel barrier, the *I*–*V* curve is nonlinear, which indicates good quality of Alq_3, since Alq_3 with pinholes would give a linear *I*–*V* curve as ill-defined layers would. Moreover, figure 2 shows very weak temperature dependence for the devices with a tunnel barrier, which is an expected behavior of the tunneling conduction. These results demonstrate that all layers are well defined and the tunneling resistance dominates the device resistance. Therefore, the external bias voltage is mainly applied across the tunnel barrier, which allows us to continuously tune the relative shift between E_F of LSMO and both HOMO and the lowest unoccupied molecular orbital (LUMO) levels of organic layer over a wide range by varying the bias voltage. In OSVs without tunnel barriers, the external bias voltage is only dropped across the organic layer, which makes HOMO/LUMO levels steeper. The current level of device 1 is about one order of magnitude larger than that of device 3, which is attributed to the smaller energy gap of $SrTiO_3$ relative to that of Al_2O_3.

The typical MR curves of device 1 are shown in figures 3(a) and (b), which were measured at 15 K. The MR ratio is defined as $MR = (R_{AP} - R_p)/R_P$. A positive bias voltage means that the voltage of the LSMO electrode is higher than that of the Co electrode. At a bias voltage $V = -0.44$ V, the MR is inverted, i.e. $R_{AP} < R_P$ and $MR < 0$ (figure 3(a)). The inverted MR is observed for $V < 0$ and the maximum MR magnitude appears at −0.3 V. For $V > 0$, the inverted MR is observed for $V < 0.5$ V but its magnitude steadily decreases as the bias voltage increases. As the bias voltage exceeds 0.5 V, MR crosses zero and turns to positive. A typical positive MR loop is shown in figure 3(b) which was measured at 0.90 V. The bias dependence over the entire voltage range is displayed in figure 3(c). The strong asymmetry in the overall bias dependence observed here is in sharp contrast from that of regular OSV without a $SrTiO_3$ tunnel barrier [1, 2, 3, 9]. Particularly, the sign change at a positive bias voltage is absent in previously studied OSVs. Furthermore, the maximum MR occurs approximately at zero bias in regular OSVs. The same qualitative bias dependence characteristics are reproduced in other devices with the nominally same structure with a tunnel barrier, although the maximum MR magnitude may vary slightly as illustrated in figure 3(c).

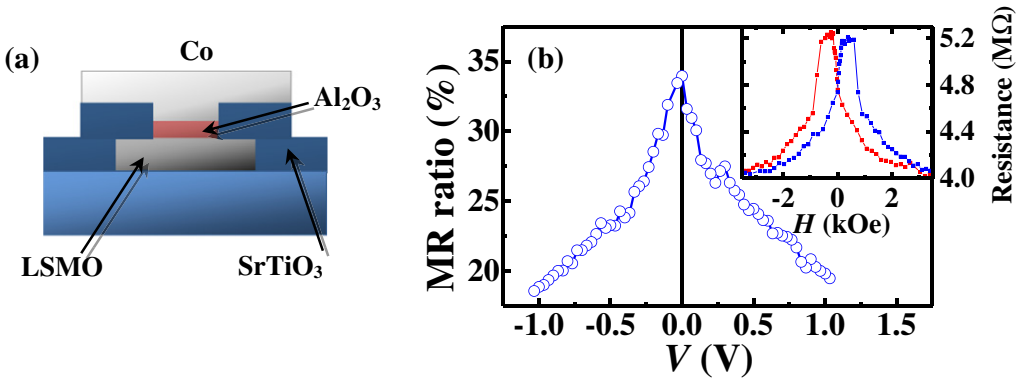

Figure 4. (a) Schematic diagrams of a LSMO/Al_2O_3/Co magnetic tunnel junction device. (b) MR ratio as a function of the applied bias voltage in LSMO/Al_2O_3(∼2.5 nm)/Co measured at 15 K. Inset: MR loop measured at 0.10 V.

The peculiar bias voltage dependence of OSV devices resembles that observed in LSMO/$SrTiO_3$/Co magnetic tunnel junction devices reported by de Teresa *et al* [20]. It also shows the maximum magnitude of inversed MR off the zero bias voltage and the MR sign reversal at a certain positive bias voltage. Considering the positive SP of LSMO at Fermi level (E_F), this behavior is generally explained by the efficient tunneling of Co d-band electrons across the Co/$SrTiO_3$ interfaces due to the interfacial d–d bonding or the complex band structure of $SrTiO_3$ [21, 22] because Co d-band SP is negative at E_F and its SP dramatically varies with energy, particularly sign reversal below E_F about 0.8 eV.

To ensure the intrinsic origin of the observed bias dependence in our OSV devices, we first eliminate some extrinsic material possibilities. As discussed earlier, the top FM metal electrode deposition frequently causes shorts especially when the OSC layer thickness is below some threshold. The resulting poor FM/OSC interfaces are likely responsible for the sign and magnitude of MR fluctuations from sample to sample as often reported [17, 18]. We believe that our indirect deposition method produces sharp Co/Alq_3 interfaces and circumvents this problem. If the Co clusters penetrated through the Alq_3 layer and made direct contacts with $SrTiO_3$, LSMO/$SrTiO_3$/Co magnetic tunnel junctions would be formed locally, which could produce the tunnel junction-like characteristics, i.e. the inverted MR and sign switching similar as observed in LSMO/$SrTiO_3$/Co. To exclude this possibility, we have carried out the following experiments. We first prepare a LSMO/Al_2O_3/Co tunnel junction device with an Al_2O_3 barrier, as shown by a schematic view of the device structure in figure 4(a). It was hypothesized that Co, when contacting with Al_2O_3, shows a positive SP in tunneling [23]. In such case, the sign of TMR in LSMO/Al_2O_3/Co is expected to be positive. Figure 4(b) shows the bias dependence in our LSMO/Al_2O_3(∼2.5 nm)/Co tunnel junction device and the inset shows a typical TMR curve. TMR is indeed positive over the entire bias range and exhibits nearly symmetric bias dependence which is in agreement with previously reported results [23].

Our second step is to fabricate OSV devices of LSMO/Al_2O_3/Alq_3/Co. We found that, upon the insertion of the Alq_3 layer between Al_2O_3 and Co, the positive and symmetric bias dependence characteristic disappears. At negative bias voltages, MR is inverted. Figure 5(a) shows a typical inverted MR loop measured on device 3 at 10 K and −0.23 V. The MR magnitude reaches its maximum at ~ -0.22 V as shown in figure 5(c). These results clearly

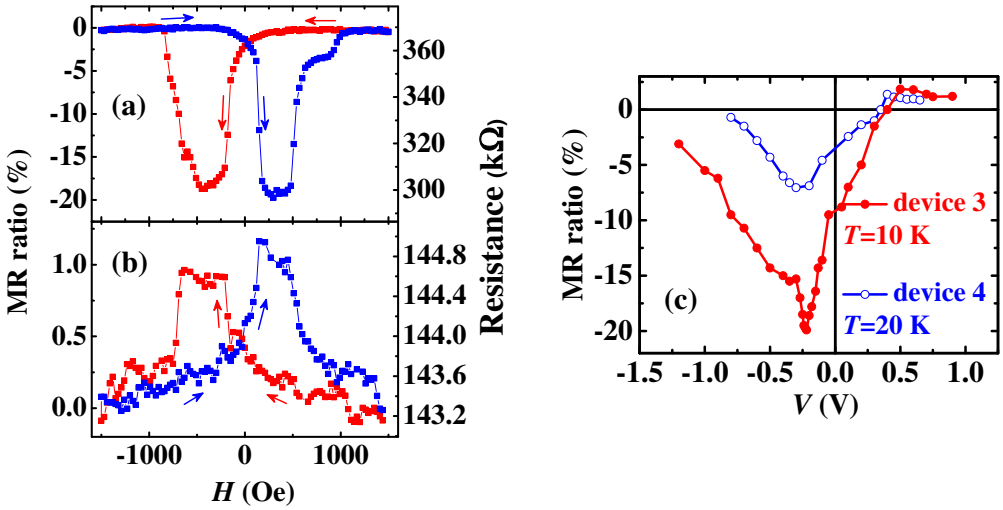

Figure 5. (a) MR loops of device 3 (with Al_2O_3 tunneling barrier) measured at 10 K with a bias voltages of −0.23 V. (b) MR loops of device 3 measured at 10 K with a bias voltage of 0.75 V. (c) MR ratio as a function of the applied bias voltage of devices 3 and 4.

demonstrate that the Co atoms or clusters do not penetrate through the 50 nm thick Alq_3 layer and reach the Al_2O_3 tunnel barrier; otherwise a positive MR with the symmetric bias dependence would have appeared as in the conventional Al_2O_3 tunnel junction shown in figure 4(b). This again proves that a significant improvement of interface between the top FM electrode and the organic layer is achieved utilizing the indirect deposition method. The 50 nm Alq_3 layer in the OSV devices with a $SrTiO_3$ barrier is also prepared with the same high quality. Hence, the pinhole-free Alq_3 layer excludes the extrinsic origin of the observed bias dependence. In LSMO/Al_2O_3/Alq_3/Co, MR reverses the sign as the bias voltage exceeds 0.4 V on the positive bias side, as represented by a typical MR loop measured at 0.75 V in figure 5(b). These features are characteristic of those found in LSMO/$SrTiO_3$/Alq_3/Co OSV devices, indicating that the OSV MR bias dependence has little to do with the tunnel barrier type, but is a property of the Co/Alq_3 interface. Figure 5(c) shows the bias dependence of two nominally same devices of LSMO (50 nm)/Al_2O_3 (∼2.3 nm)/Alq_3(50 nm)/Co(20 nm)/Al(15 nm) (devices 3 and 4) at 10 and 20 K, respectively. Despite the difference in the absolute MR ratio, the qualitative bias dependence follows the same characteristic trend as in the $SrTiO_3$ devices. These facts suggest that the unique MR bias dependence characteristic originates from the top Co/Alq_3 interface, the common interface in both types of samples, not from the tunneling interface at the bottom. Since LSMO has nearly 100% SP near its Fermi level and therefore has no energy dependence, we attribute the observed complex bias dependence in MR to the electronic properties of d-electrons of Co/Alq_3.

As shown earlier, adding a 50 nm thick Alq_3 does not increase the total resistance significantly. We also know that OSV devices with a 50 nm thick Alq_3 have relatively low resistance. It is consistent with the general belief that the injected spin-polarized carriers transport through the OSC layer via hopping before reaching the other FM electrode. The actual band alignment and effective thickness of the OSC layer may affect the resistance and even the overall magnitude of MR over a range of bias voltages, but should not determine the MR bias

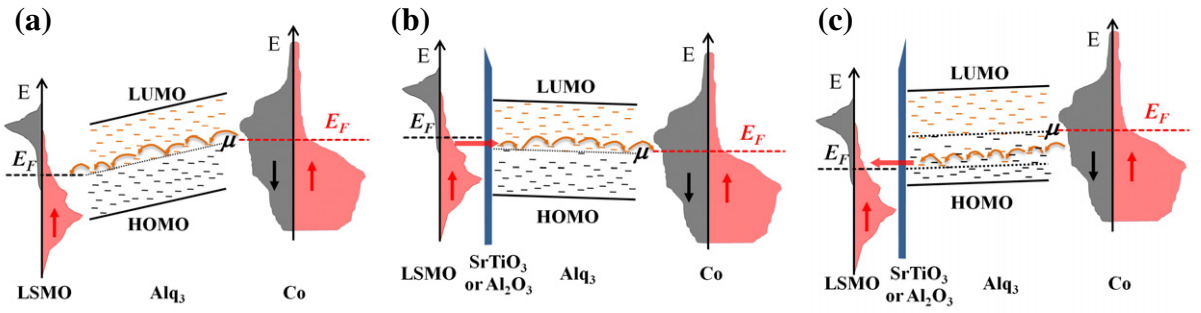

Figure 6. The energy-level diagrams for (a) LSMO/Alq_3/Co with a positive bias voltage, LSMO/tunnel barrier/Alq_3/Co with (b) a negative bias voltage and (c) a positive bias voltage.

dependence. Based on this picture, our bias dependence results can be understood by the Co unique d-band DOS.

We can further understand the correlation of the MR bias dependence with the Co d band in terms of the energy-level diagrams in figure 6. The low resistance level strongly suggests that the carriers transport through the intra-gap states between HOMO and LUMO instead of the HOMO and LUMO levels themselves because a much larger resistance level would be resulted from injecting carriers from/to E_F of electrodes to/from HOMO or LUMO level at low bias voltages. And the abundant intra-gap states in Alq_3 induced by the deposition of Co were recently observed by ultraviolet photoelectron spectra [24] This intra-gap hopping transport mechanism has been adopted by various groups [25, 26]. Figure 6(a) shows the energy level diagram of LSMO/Alq_3/Co OSV device with a positive bias voltage. The voltage is dropped across the Alq_3 layer. The electrons at Co E_F inject into Alq_3 and then hop through the gap states in the Alq_3 layer to arrive at LSMO electrode. The gap states are occupied below the chemical potential of Alq_3, μ, which is aligned with the E_F of two electrodes at interfaces. The electrons can only hop between the vacant gap states around μ, indicating that only states around E_F of two electrodes contribute to transport. Since the SP of LSMO and Co is opposite at E_F, the sign of MR is negative and it is independent of bias voltages.

For OSVs with a tunnel barrier, $SrTiO_3$ or Al_2O_3, the tunneling dominates the resistance of OSVs. Therefore, the external bias voltage is mainly dropped across the tunnel barrier instead. The relative energy level alignment between LSMO and Alq_3 are set by the bias voltage, as shown in figures 6(b) and (c). At negative bias voltages, the electrons of LSMO, whose energy is higher than μ, tunnel across the barrier and then hop through the gap states in the Alq_3 layer to arrive at the Co unoccupied d-states (figure 6(b)). Since the Co spin-down DOS is higher than Co spin-up DOS and shows a peak above E_F, the MR has a negative sign with a MR ratio peak at a negative bias voltage. At positive bias voltages, the Co d-state electrons, whose energy is higher than LSMO E_F, inject into and then hop through the Alq_3 layer and tunnel across the barrier to arrive at the LSMO unoccupied states (figure 6(c)). Below Co E_F, spin-up DOS increase and spin-down DOS decrease progressively, indicating that more spin-down electrons and the fewer spin-down electrons are injected into the Alq_3 as the bias voltage gradually increases. Eventually, when the bias voltage is above $\sim$0.4 V, more spin-up electrons are injected into the Alq_3 than spin-up electrons, namely, Co shows an effective positive SP and consequently, a positive MR is resulted.

To understand the Co/Alq_3 interface, we have performed *ab initio* calculations of the electronic structure of hcp Co(0001) surface with an Alq_3 molecule adsorbed, based on the density functional theory in the Perdew–Burke–Ernzerhof generalized gradient approximation (GGA) [27], using the Vienna *ab initio* simulation package code with projector augmented wave pseudopotentials [28, 29]. In our devices, Co is polycrystalline therefore must contain grains in all orientations. Here we choose the lowest energy surface in hcp Co, i.e. (0001) orientation as an example. In our calculations, an energy cutoff of 550 eV is used for expanding the Kohn–Sham wave functions. A slab consisting of three-layer Co atoms in hcp (0001) arrangement is used to model the Co (0001) surface. There are two isomers of the Alq_3 molecule, facial and meridional. Since the meridional isomer is much more stable [30], we calculate one meridional isomer on Co (0001) surface and allow the uppermost two Co layers and the molecule to relax. The Alq_3 structure is finally obtained until the atomic force is lower than 0.01 eV $Å^{-1}$. The stable adsorption geometry of the Alq_3 molecule on Co surface is shown in figure 7(a). Two of the quinoline ligands (L_A and L_B) lie on the Co surface, and the third ligand (L_C) is oriented perpendicular to the surface. Note that the ligands L_A and L_B are strongly twisted and turn to be non-planar. The strongest interaction between the Alq_3 molecule and the substrate occurs at the O atom of ligand L_C, with the shortest O–Co bond length of 1.9 Å, compared with the other atoms that are further away (i.e. 2.0 up to 7.5 Å) from Co atoms. It indicates that the binding between Co and Alq_3 is dominated by the O–Co bond, which is in agreement with the recent x-ray photoelectron spectroscopy results and theoretical calculations [30, 31]. The shortest bond lengths for N and C atoms with Co are 2.0 and 2.8 Å, respectively. The isosurface plot of the charge density in figure 7(a) clearly illustrates the strongest bond between the O in L_C of Alq_3 and Co atoms.

The calculated energy gap between HOMO and LUMO for free Alq_3 is about 2.3 eV, which is in agreement with the experimental value of 2.8 eV [31, 32], considering the fact that GGA tends to underestimate the band gap of materials. The remarkable geometrical distortion as a result of the interface chemical interactions significantly affects the electronic structure of Alq_3 molecule, as can be seen from the local partial density-of-states (LPDOS) of the O, N and C atoms which are closest to Co, depicted in figure 7(b), respectively. Owing to the geometrical distortion, not only the out-of-plane π-type p_z states but also the in-plane σ-type s, p_x and p_y states develop strong delocalized characteristics, as manifested by the smooth and broad bands without an energy gap [33]. In contrast, for planar molecules lying flat onto the substrates, the molecular π-orbitals usually hybridize with metal surface much more strongly than molecular σ-orbitals [34]. The most interesting consequence of the hybridization with FM atoms is the formation of the exchange-split states, similar to other molecules chemically adsorbed on FM surfaces [33, 34]. Again owing to the shortest bonding and thus the strongest interfacial hybridization, the O atom shows the highest LPDOS and the largest SP around E_F than the C and N atoms. Therefore, the O–Co bond should dominate the electron injection from Co to Alq_3 since the hopping integral from Co to Alq_3 is directly correlated with the hybridization strength [35].

For comparison, we present in figure 7(b) the calculated LPDOS for a Co atom on a clean Co surface and the Co atom with the shortest bond with O upon absorbing Alq_3. Apparently, the shape of the out-of-plane d-states (d_{z2}, d_{xz}, d_{yz}) of Co in both spin channels is drastically altered after the absorption of Alq_3, particularly around E_F. In contrast, the shape of the in-plane d-states (d_{x2+y2}, d_{xy}) of Co is less affected. It reflects stronger interfacial hybridization of the π-bond of Co atom with Alq_3 than the σ-bond counterpart. In addition, the s-state does not show

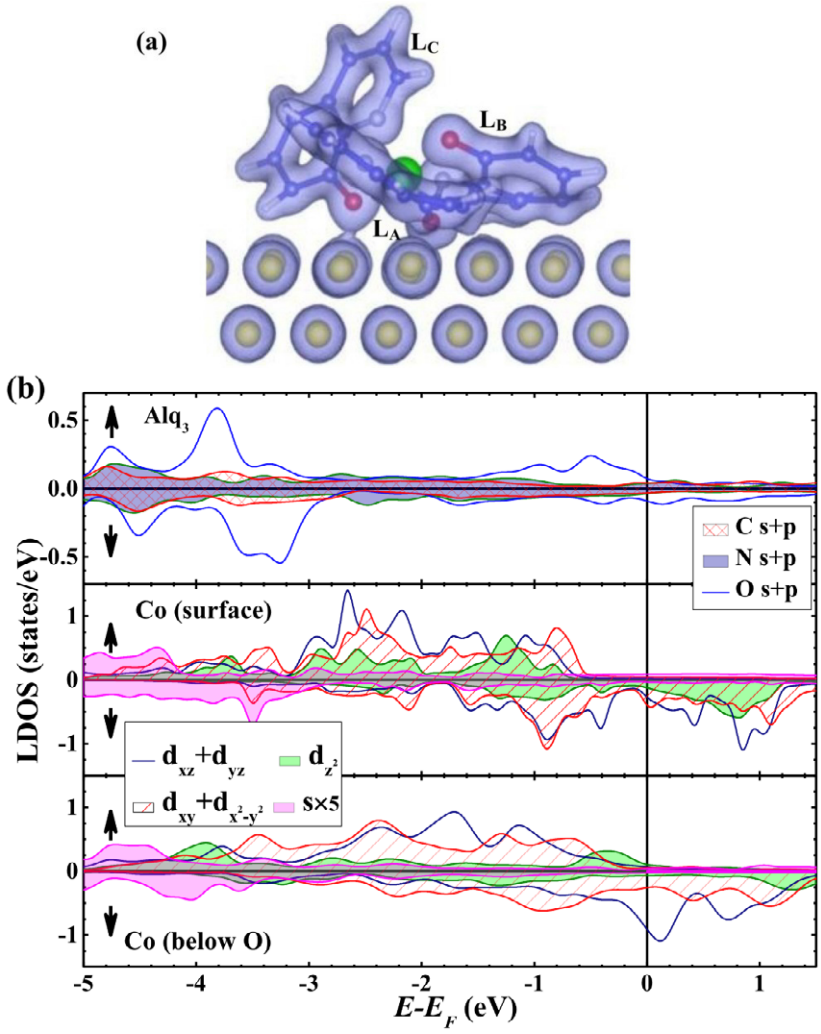

Figure 7. (a) The schematic visualization of the Alq_3 molecule adsorbed on Co surface with the optimized geometry, the calculated electron density iso-surface is shown in blue (isovalue: 10^5 nm^{-3}). The atoms are shown in different colors: Al, green; O, red; N, gray; C, blue; H, white; Co, yellow. (b) Calculated spin-resolved LPDOS of the Alq_3 on a Co surface for the C, N and O atoms which are closest to Co, and a Co atom of the clean surface and the Co atom with the shortest bond with O, respectively.

significantly change around E_F and the LPDOS is one order of magnitude smaller than that of the d-states, suggesting that the d–p bonding is much stronger than s–p bonding between Alq_3 and Co. Importantly, the hybridization strength is correlated with the spin injection efficiency.

Although the SP of LSMO was measured by different techniques to vary widely from ∼35 to ∼100%, the experiments suggested a positive SP [36–38]. The magnitude of SP only influences the MR ratio not the MR sign. Owing to the positive SP over a relatively large energy range in LSMO, the sign of MR is dictated by the sign of SP at the Co/Alq_3 interface based on the Jullière model [14]. The interfacial injection efficiency depends on the hopping integrals between the electrodes and the molecules, which are directly determined by the interfacial hybridization, resulting in the band selected injection. The interfacial bonding plays the same essential role as in inorganic spintronics [20, 21]. We note that the detail Co band structure

may be related with the absorbed Alq_3 structure. However, it would not change the fact that the p–d hybridization is stronger than p–s hybridization due to much higher d band LPDOS. Therefore, the spin injection dominated by Co d band is not sensitive to the molecule structure. Since the out-of-plane d states of Co have the strongest hybridization with Alq_3, they should dominate spin injection into Alq_3. Around E_F, the SP of the out-of-plane states is negative; therefore, it gives rise to a negative MR at low bias voltages, which is in good agreement with our experimental observations. In addition, the LPDOS of unoccupied out-of-plane spin-down d-states, which is responsible for the electrons extraction from Alq_3 to Co at negative bias, shows a peak around 0.1 eV. This peak explains the maximum MR magnitude observed in the same bias range. Below E_F, the LPDOS of spin-up states is higher than spin-down states and shows a peak at round -0.4 eV. It corresponds to the MR sign reversal at positive bias voltages in our experimental data. Although only Alq_3 absorbed on Co hcp (0001) surface is calculated, we believe that the strong p–d hybridization between Alq_3 and Co should be a general property of the interface. If s–p or p–p bonding is preferred in real devices, a positive SP and simpler bias dependence would be resulted.

4. Conclusion

In summary, we demonstrated that the interface between the top FM electron and the organic layer can be significant improved via the newly developed indirect deposition method. By inserting a thin tunnel barrier in conventional OSVs, we showed that one can tune the band alignment over a wide range of energies of Co electronic structure. Consequently, we discovered a reproducible and strong asymmetric bias dependence in LSMO/$SrTiO_3$(or Al_2O_3)/Alq_3/Co OSV devices. The MR exhibits a negative maximum value at a negative bias and turning positive at a certain positive bias voltage. Together with the first-principle calculations, we identified this unique bias dependence is originated from the energy dependent DOS of Co d-states, similar as the finding in inorganic spintronic devices. The finding also suggested the origin of the inverse MR phenomenon observed in ordinary LSMO/Alq_3/Co OSV devices originated from negative SP of Co at E_F. Our results open up new possibilities to engineer interfacial bonding between FM materials and a wide variety of molecule selections for the desired spin transport properties.

Acknowledgments

This work was supported by the National Basic Research Program of China (2010CB923402, 2013CB922103, 2010CB30705 and 2012CB921502), NSF of China (11222435, 11174123, 10974084, 11023002 and 11034005), NCET project (NCET-09-0461), the Priority Academic Program Development of Jiangsu Higher Education Institutions and the Fundamental Research Funds for the Central Universities. JS at UCR was supported by a US DOE award (#DE-FG02-07ER46351).

References

[1] Xiong Z H, Wu D, Vardeny Z V and Shi J 2004 *Nature* **427** 821
[2] Prezioso M, Riminucci A, Bergenti I, Graziosi P, Brunel D and Dediu V A 2011 *Adv. Mater.* **23** 1371
[3] Nguyen T D, Ehrenfreund E and Vardeny Z V 2012 *Science* **337** 204
[4] Dediu V A, Hueso L, Bergenti I and Taliani C 2009 *Nature Mater.* **8** 707

[5] Majumdar S, Majumdar H S, Laiho R and Österbacka R 2009 *New J. Phys.* **11** 013022
[6] Naber W J M, Faez S and van der Wiel W G 2007 *J. Phys. D: Appl. Phys.* **40** R205
[7] Szulczewski G, Sanvito S and Coey M 2009 *Nature Mater.* **8** 693
[8] Sanvito S 2011 *Chem. Soc. Rev.* **40** 3336
[9] Sun D L, Yin L F, Sun C J, Guo H W, Gai Z, Zhang X G, Ward T Z, Cheng Z H and Shen J 2010 *Phys. Rev. Lett.* **104** 236602
[10] Lin R, Wang F, Rybicki J, Wohlgenannt M and Hutchinson K A 2010 *Phys. Rev.* B **81** 195214
[11] Barraud C *et al* 2010 *Nature Phys.* **6** 615
[12] Santos T S, Lee J S, Migdal P, Lekshmi I C, Satpati B and Moodera J S 2007 *Phys. Rev. Lett.* **98** 016601
[13] Dediu V *et al* 2008 *Phys. Rev.* B **78** 115203
[14] Julliere M 1975 *Phys. Lett.* A **54** 225
[15] Schulz L *et al* 2011 *Nature Mater.* **10** 39
[16] Shi Y J, Zhou Y, Ding H F, Zhang F M, Pi L, Zhang Y H and Wu D 2012 *Appl. Phys. Lett.* **101** 122409
[17] Vinzelberg H, Schumann J, Elefant D, Gangineni R B, Thomas J and Buüchner B 2008 *J. Appl. Phys.* **103** 093720
[18] Jiang J S, Pearson J E and Bader S D 2008 *Phys. Rev.* B **77** 035303
[19] Wang S, Shi Y J, Lin L, Chen B B, Yue F J, Du J, Ding H F, Zhang F M and Wu D 2011 *Synth. Met.* **161** 1738
[20] De Teresa J M, Barthélémy A, Fert A, Contour J P, Lyonnet R, Montaigne F, Seneor P and Vaurès A 1999 *Phys. Rev. Lett.* **82** 4288
[21] Tsymbal E Y and Pettifor D G 1997 *J. Phys.: Condens. Matter* **9** L411
[22] Velev J P, Belashchenko K D, Stewart D A, van Schilfgaarde M, Jaswal S S and Tsymbal E Y 2005 *Phys. Rev. Lett.* **95** 216601
[23] De Teresa J M, Barthélémy A, Fert A, Contour J P, Montaigne F and Seneor P 1999 *Science* **286** 507
[24] Xu W, Brauer J, Szulczewski G, Driver M S and Caruso A N 2009 *Appl. Phys. Lett.* **94** 233302
[25] Riminucci A, Prezioso M, Pernechele C, Graziosi P, Bergenti I, Cecchini R, Calbucci M, Solzi M and Dediu V A 2013 *Appl. Phys. Lett.* **102** 092407
[26] Alam K M, Bodepudi S C, Starko-Bowes R and Pramanik S 2012 *Appl. Phys. Lett.* **101** 192403
[27] Perdew J P, Burke K and Ernzerhof M 1996 *Phys. Rev. Lett.* **77** 3865
[28] Blöchl P E 1994 *Phys. Rev.* B **50** 17953
[29] Kresse G 1999 *Phys. Rev.* B **59** 1758
[30] Wang Y P, Han X F, Wu Y N and Cheng H P 2012 *Phys. Rev.* B **85** 144430
[31] Zhan Y Q, de Jong M P, Li F H, Dediu V, Fahlman M and Salaneck W R 2008 *Phys. Rev.* B **78** 045208
[32] Lee S T, Hou X Y, Mason M G and Tang C W 1998 *Appl. Phys. Lett.* **72** 1593
[33] Brede J, Atodiresei N, Kuck S, Lazić P, Caciuc V, Morikawa Y, Hoffmann G, Blügel S and Wiesendanger R 2010 *Phys. Rev. Lett.* **105** 047204
[34] Javaid S *et al* 2010 *Phys. Rev. Lett.* **105** 077201
[35] Raman K V, Watson S M, Shim J H, Borchers J A, Chang J and Moodera J S 2009 *Phys. Rev.* B **80** 195212
[36] Park J H, Vescovo E, Kim H J, Kwon C, Ramesh R and Venkatesan T 1998 *Phys. Rev. Lett.* **81** 1953
[37] Nadgorny B 2007 *J. Phys.: Condens. Matter* **19** 315209
[38] Nadgorny B, Mazin I I, Osofsky M, Soulen R J Jr, Broussard P, Stroud R M, Singh D J, Harris V G, Arsenov A and Mukovskii Ya 2001 *Phys. Rev.* B **63** 184433